Supporting Information

Mechanism and Selectivity of MOF-Supported Cu Single-Atom Catalysts for the Preferrential CO Oxidation

Sarawoot Impeng[1], Evaristo Salaya-Gerónimo[2], Benny Kunkel,[2] Stephan Bartling,[2] Kajornsak Faungnawakij,[1] Bunyarat Rungtaweevoranit,[1] Ali M. Abdel-Mageed [2✉]

[1]*National Nanotechnology Center (NANOTEC), National Science and Technology Development Agency (NSTDA), Pathum Thani 12120, Thailand*
[2]Leibniz-Institut für Katalyse *(LIKAT), D-18059, Rostock, Germany*

Table of Contents:

Supporting Tables:

Table S1. Summary of structural characteristic of the Cu/UiO-66

Catalyst	Cu loading (wt. %)[a]	Cu/Zr_6[a]	BET surface area (m^2/g)
UiO-66	-	-	1561
Cu/UiO-66	2.0	0.8	1511

[a] Determined by ICP analysis

Table S2. Fit parameters of EXAFS data collected during CO oxidation (COX) at different temperatures (250, 180 and 120 °C).

Measurement	CN	DWF / $Å^{-2}$	R / Å	E_0
H250	2.0 ± 0.5	0.00228 ± 0.001	1.98 ± 0.02	-14.307 ± 0.6

CN: Cu-O first shell coordination number. σ^2: mean square displacement, which is included in the Debye-Waller-Factor (DWF) according to this expression [exp $(-2\sigma^2 k^2)$]; with k being the wave vector. R: Cu-O bond distance. E_0: energy reference parameter. In these fits, the amplitude correction factor (S_0^2) was kept at a value between 0.85, which was determined from the calibration of the experimental references by FEFF models. For CN numbers in the range given the quality of the fit essentially did not change, while outside it decreased measurably. Therefore, we prefer to give ranges for CN rather than error bars.

Table S3 The effect of confinement on the adsorption energy and activation energy barrier.

Reaction species	Zr-acetate cluster	Zr-benzoate cluster
II	-122 kJ/mol	-120 kJ/mol
III	-154 kJ/mol	-159 kJ/mol
TS I	-60 kJ/mol (E_a = 94 kJ/mol)	-63 kJ/mol (E_a = 96 kJ/mol)

To investigate the effect of confinement on the adsorption energy and activation energy barrier, we did test calculations by using benzoate groups as linkers. We calculated the adsorption energies of O_2 (intermediate **I**), H_2/O_2 co-adsorption (intermediate **II**), and the energy barrier for **TS I** on the triplet spin state. As shown in Table S3, the adsorption energies and energy barrier calculated with benzoate groups are similar to those obtained with acetate groups. This suggests that increasing the size of the catalyst model to account for the confinement effect of UiO-66 MOF, does not significantly alter the calculated adsorption energies and activation energy barrier of small molecules such as O_2 and H_2.

Additional results

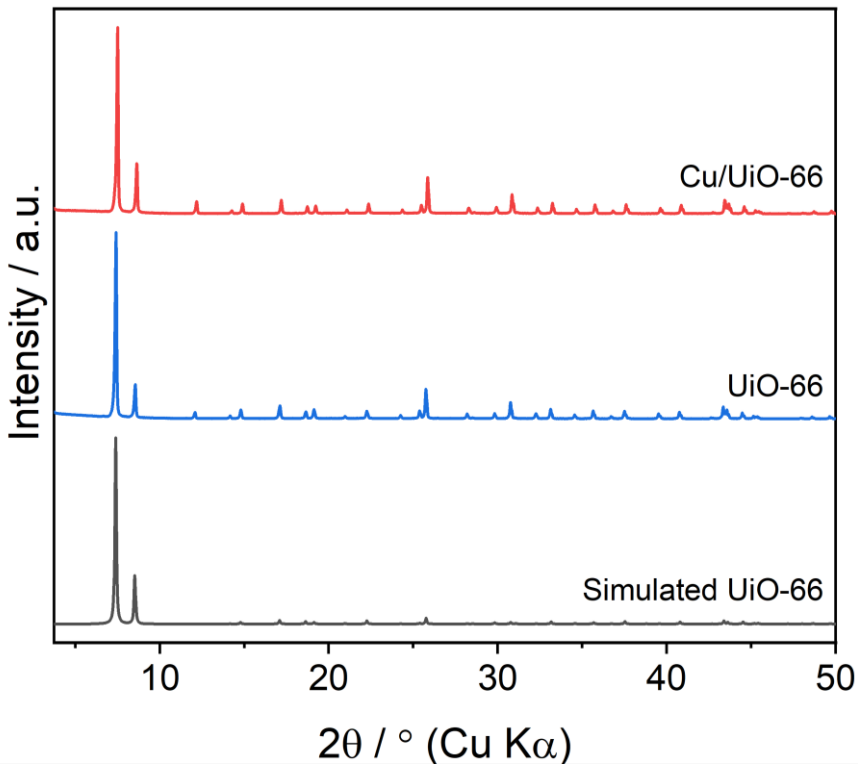

Figure S1. PXRD of UiO-66 and Cu/UiO-66 overlaid with the simulated pattern of UiO-66.

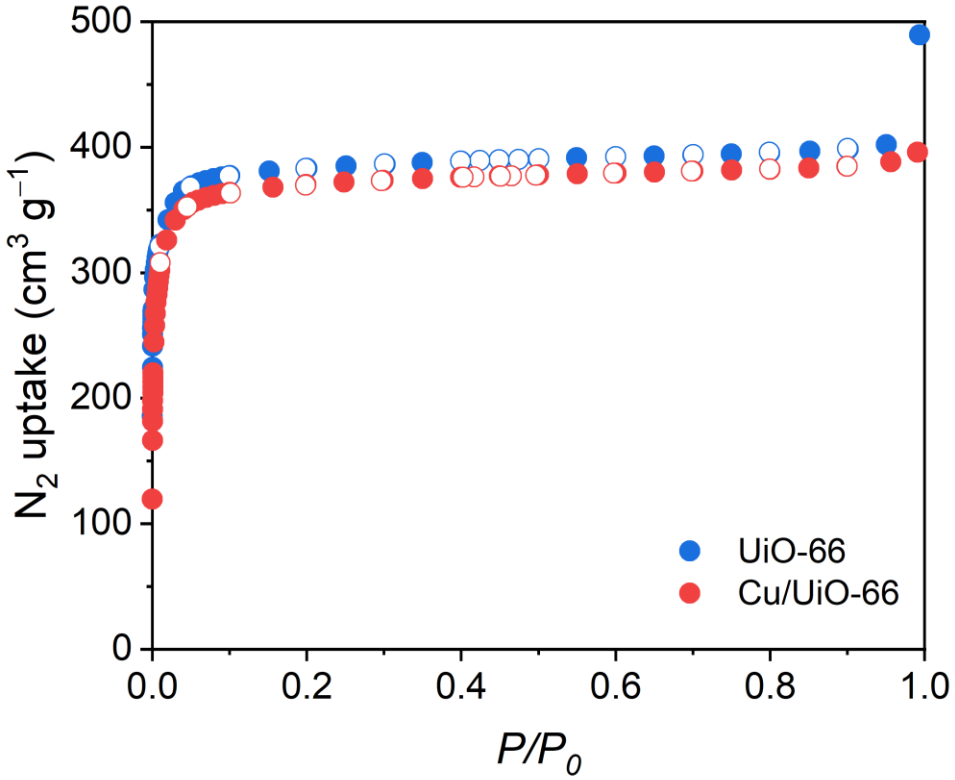

Figure S2. N_2 adsorption-desorption isotherms recorded at 77 K of UiO-66 and Cu/UiO-66.

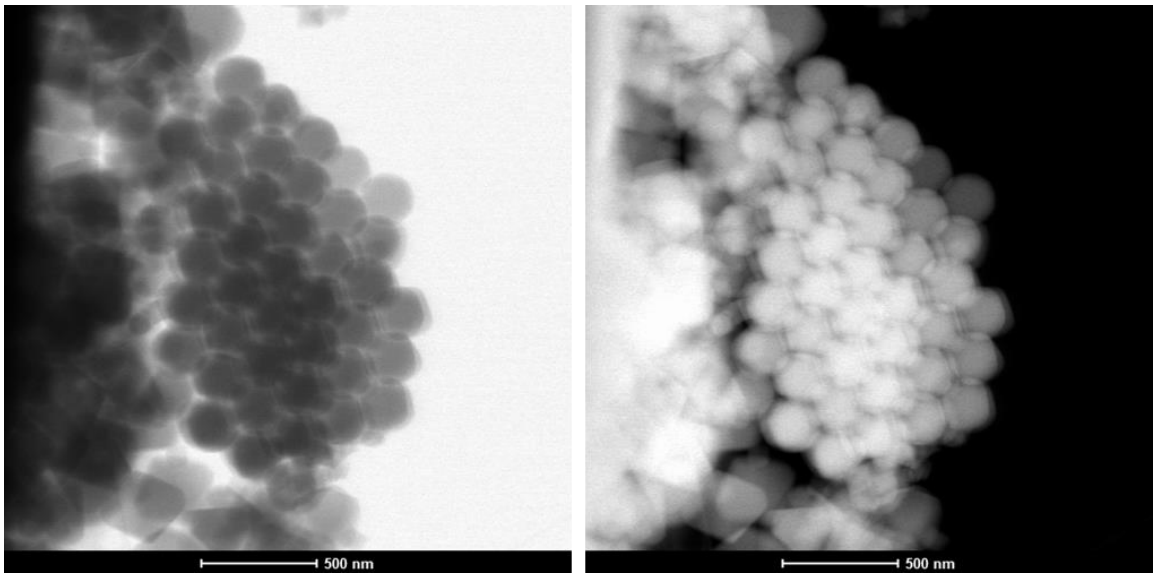

Figure S3. Bright and dark field scanning transmission electron microscopy (a: BF-STEM; b: HAADF STEM) results of the fresh reduced Cu1/UiO-66 catalyst.

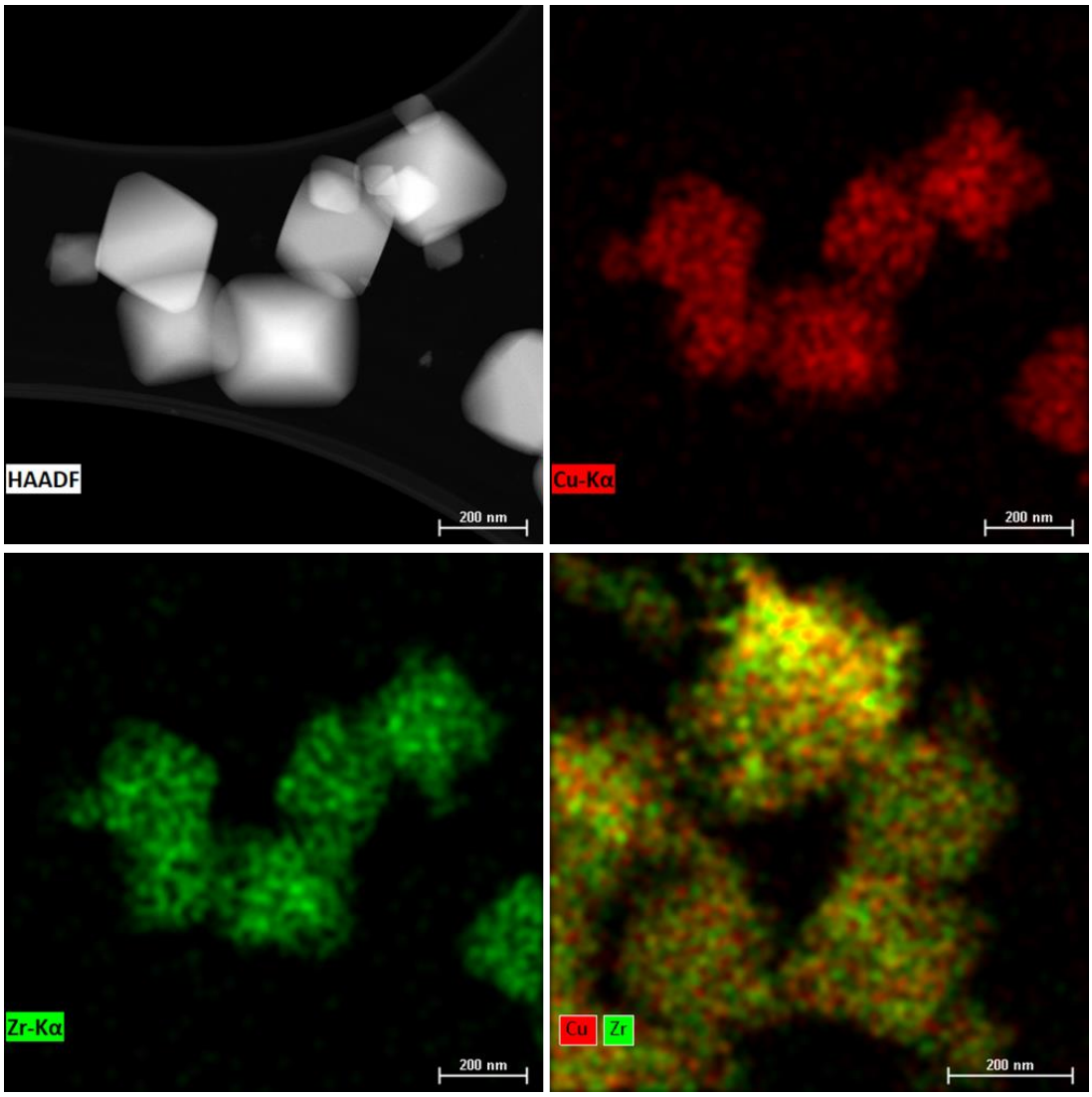

Figure S4. HADDF STEM (a) micrograph and corresponding EDS maps of Cu(b), Zr (c) and the hybrid Cu/Zr map (d) of the Cu1/UiO-66 after H250 treatment.

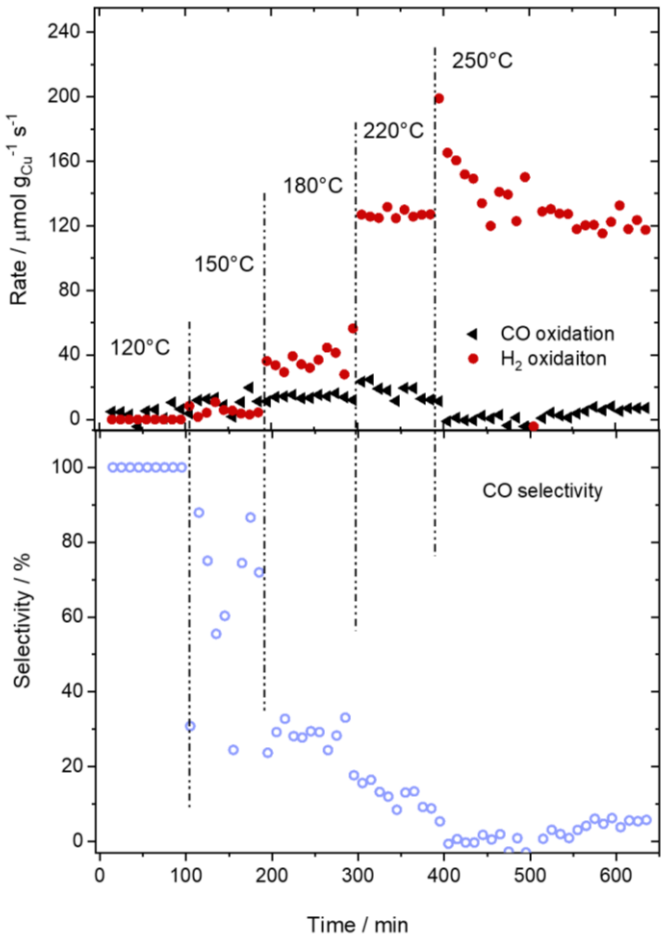

Figure S5. (a) Reaction rates for the oxidation of CO and H_2 PROX reaction (1% CO, 1% O_2, 80% H_2 and N_2) on Cu/UiO-66 catalyst (prepared by solvothermal method)at different temperatures with time on stream, after the H250 pretreatment (1 h in 10% H_2/Ar at 250°C) and (b) corresponding selectivity changes. Calculated gas hourly space velocity (GHSV) = 10975 h^{-1}.

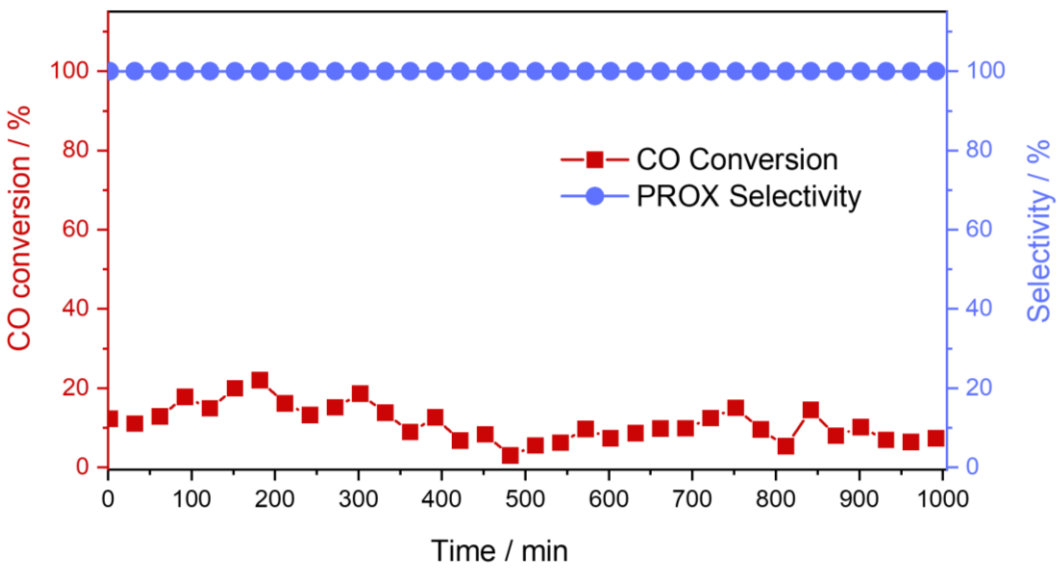

Figure S6. Time-on-stream CO oxidation activity and corresponding PROX selectivity (as measured CO conversion) on Cu1/UiO-66 catalyst (prepared by solvothermal method) during PROX reaction (1% CO, 1% O_2, 80% H_2 and Ar) at 120°C directly after the H250 pretreatment (1 h in 10% H_2/Ar at 250°C). Calculated gas hourly space velocity (GHSV) = 3658 h^{-1}.

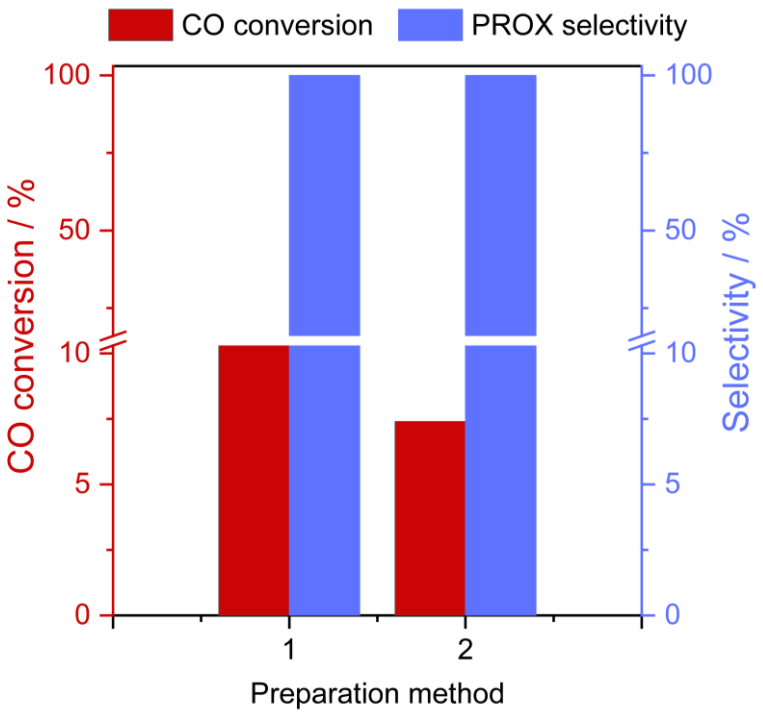

Figure S7. Comparison of the steady state CO conversion and corresponding PROX selectivity prepared on Cu1/UiO-66 catalysts by solvothermal method (1) and using mechanical mixing method (2) during PROX reaction (1% CO, 1% O_2, 80% H_2 and Ar) at 120°C directly after the H250 pretreatment (1 h in 10% H_2/Ar at 250°C). Calculated gas hourly space velocity (GHSV) = 3658 h^{-1}.

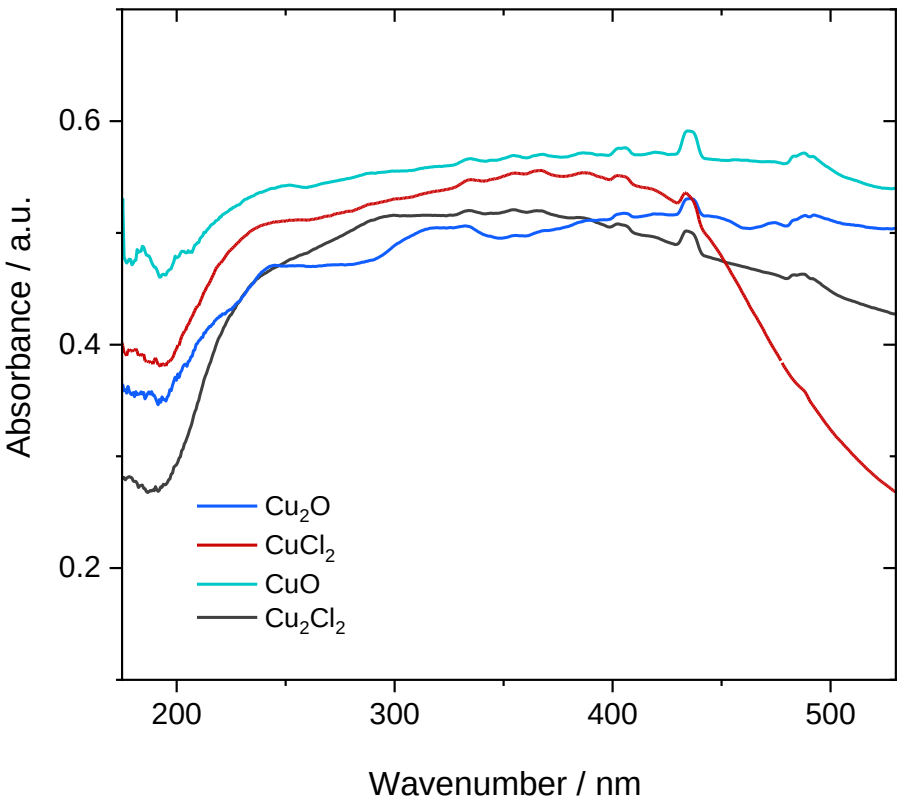

Figure S8. Measured spectra of different reference materials of Cu(I) and Cu(II) recorded under flow of Ar at room temperature.

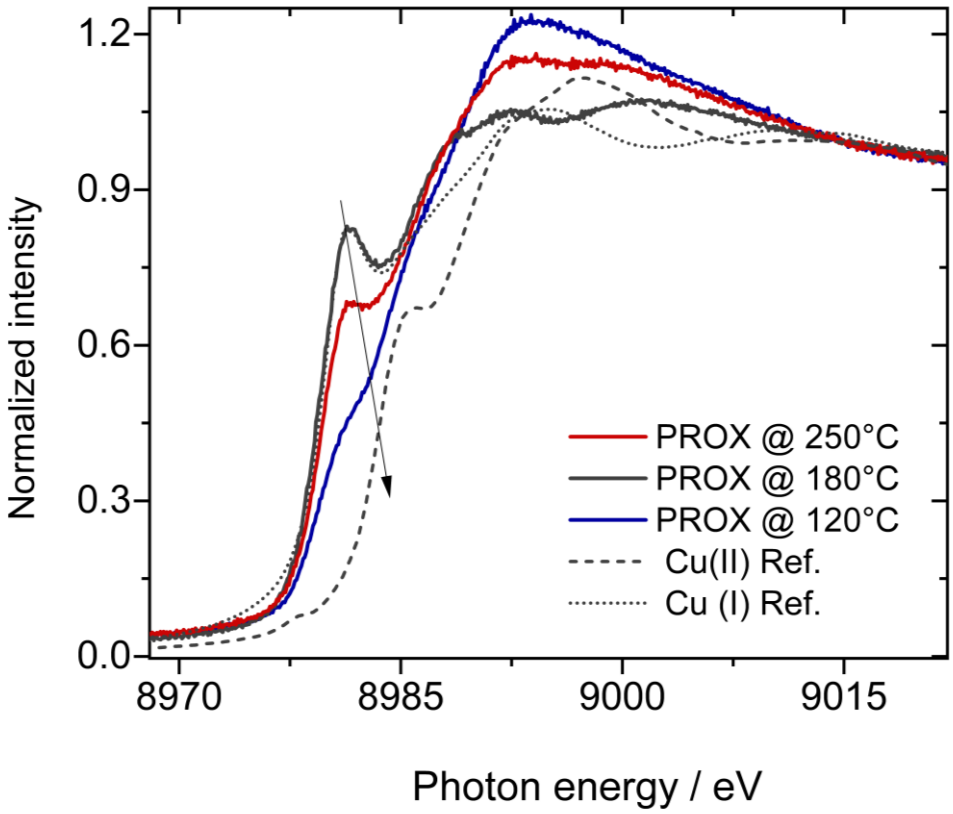

Figure S9. Cu K-edge XANES spectra recorded during PROX reaction at different temperatures in standard gas mixture (1% CO, 1% CO, 80% H_2, balance N_2) compared to reference spectra for Cu(I) and Cu (II) ions taken on Cu2O and CuO powders.

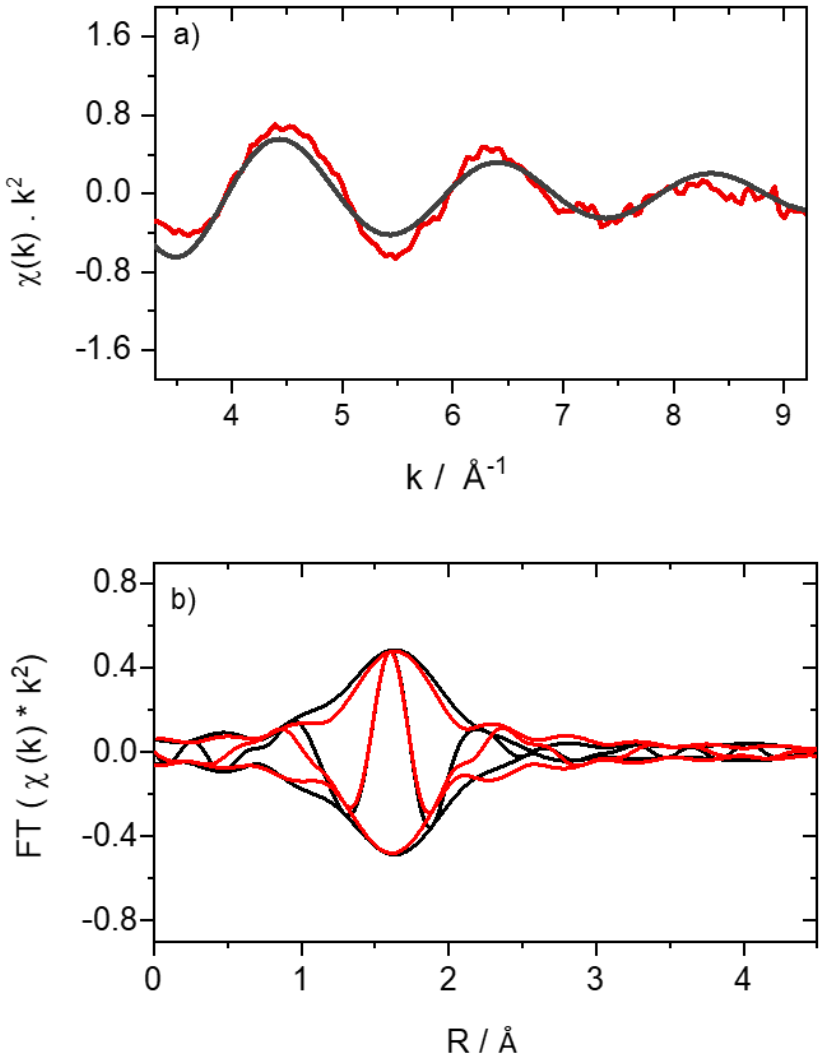

Figure S10. EXAFS spectra after the reductive treatment of Cu/UiO-66 in hydrogen at 250°C

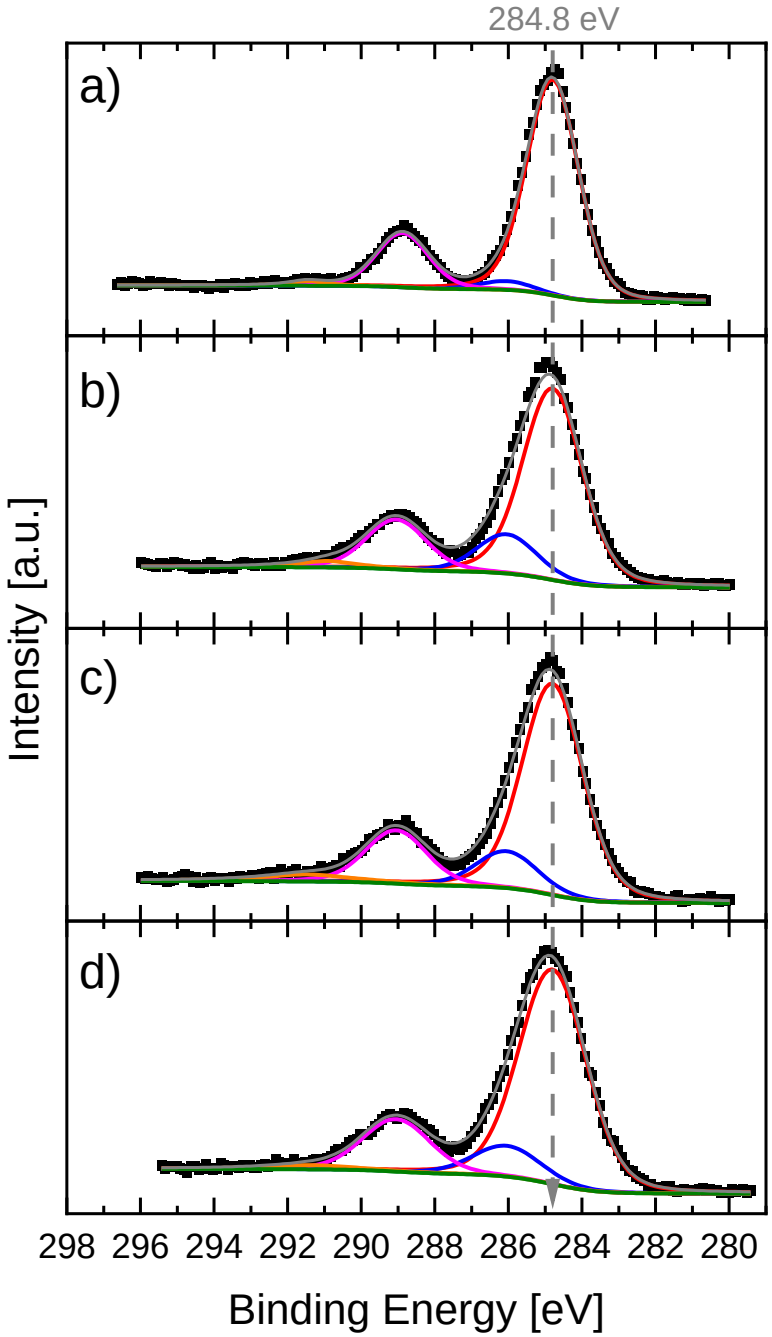

Figure S11. NAP-XP spectra for the C1 region at 250°C and a pressure 2 mbar and different feed gases (a, e: in He after heating from RT; b, f: in 10% H_2/He; c, g: in PROX gas (1% CO, 1%O_2, 80% H_2, He balance); d, h: back again in He).

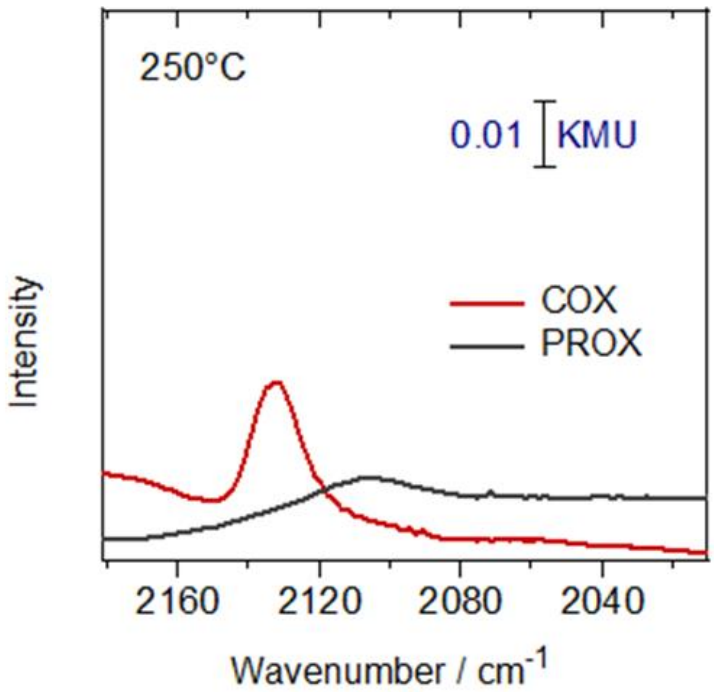

Figure S12. CO_{ad} bands during preferential CO oxidation (1%CO, 1% O_2, 80% and N_2 balance) and CO oxidation (1%CO, 1% O_2, 80% and N_2 balance) at 250°C°C.

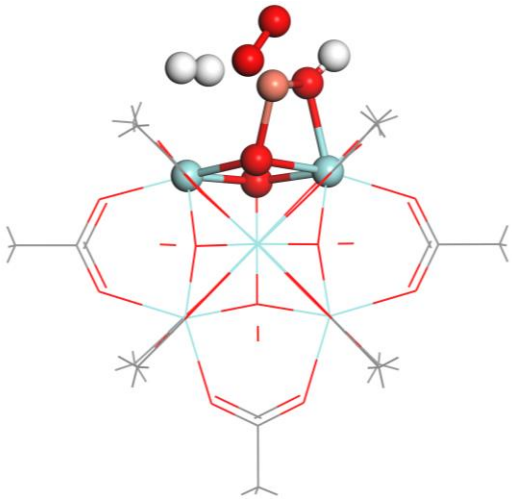

Figure S13. The optimized structure of co-adsorption configuration of O_2 and H_2 with the adsorbed O_2 on Cu site.

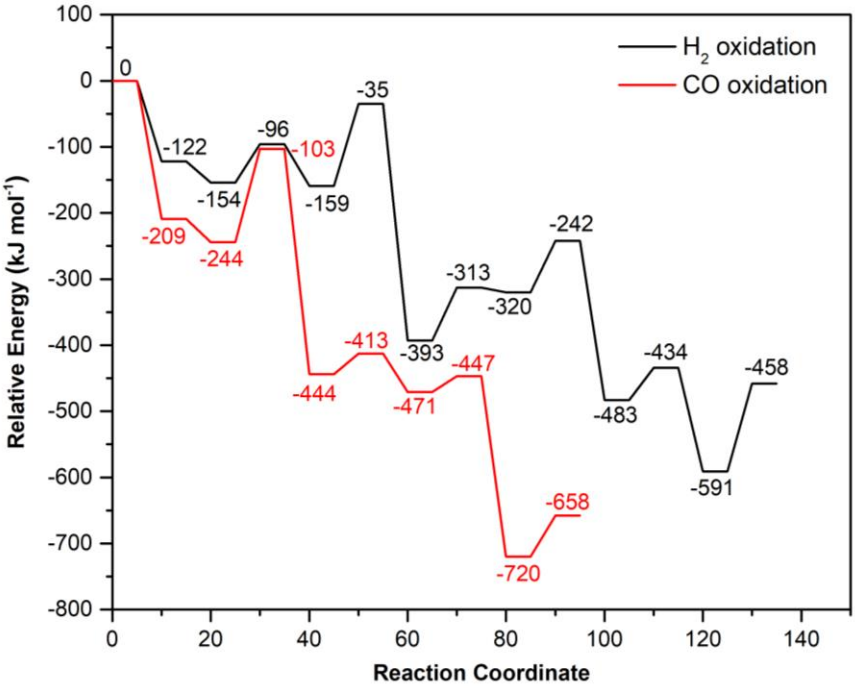

Figure S14. Comparison of the energy profile of the CO and H_2 oxidation

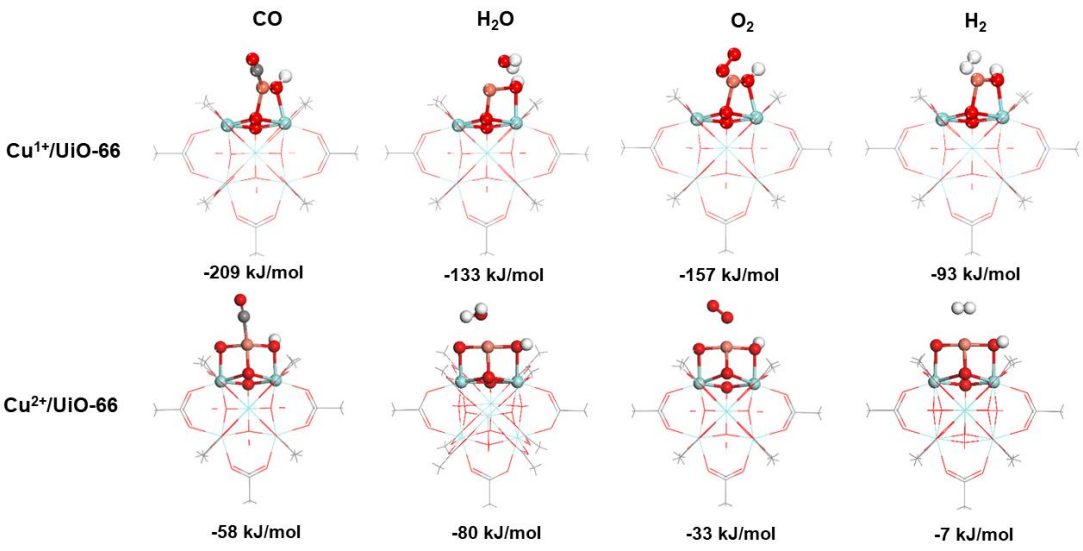

Figure S15. The optimized structures of the most stable adsorption of CO, H_2O, O_2 and H_2 on the Cu^{1+} and Cu^{2+} sites.

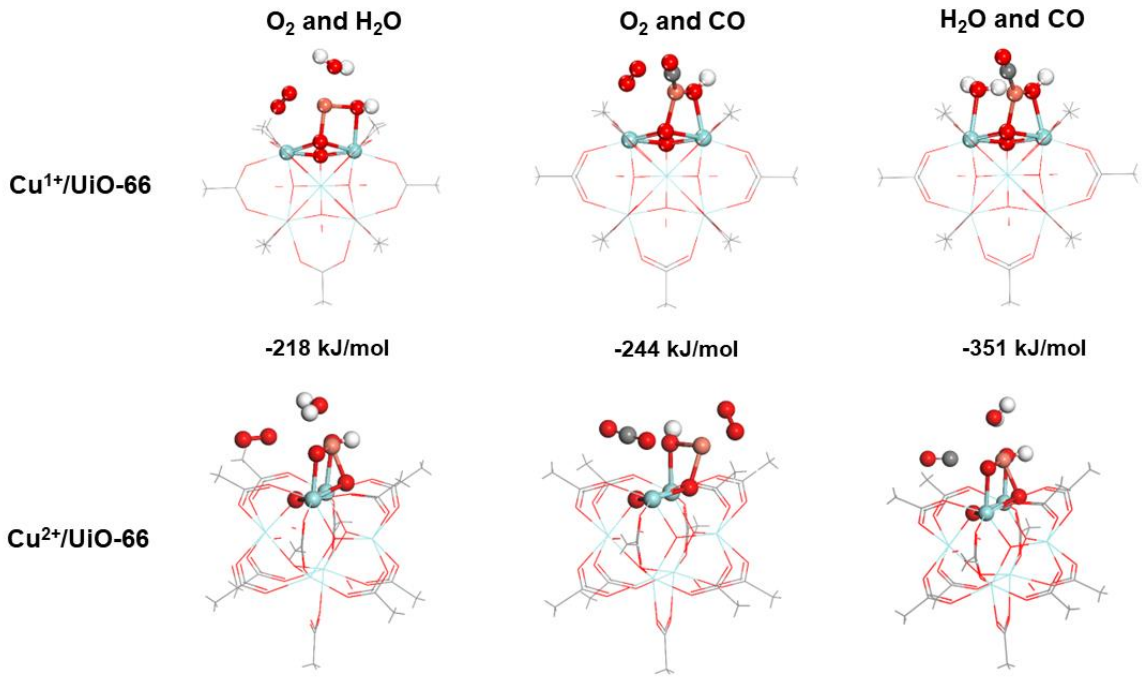

Figure S16. The optimized structures of the most stable co-adsorption of O_2/H_2O, O_2/CO and H_2O/CO on the Cu^{1+} and Cu^{2+} sites.

We note here that the optimization of CO and O_2 co-adsorption on the Cu^{2+} site results in co-adsorption of CO_2 and O_2 on the Cu^{1+} site according to the CO oxidation by the adsorbed O_{br} atom.

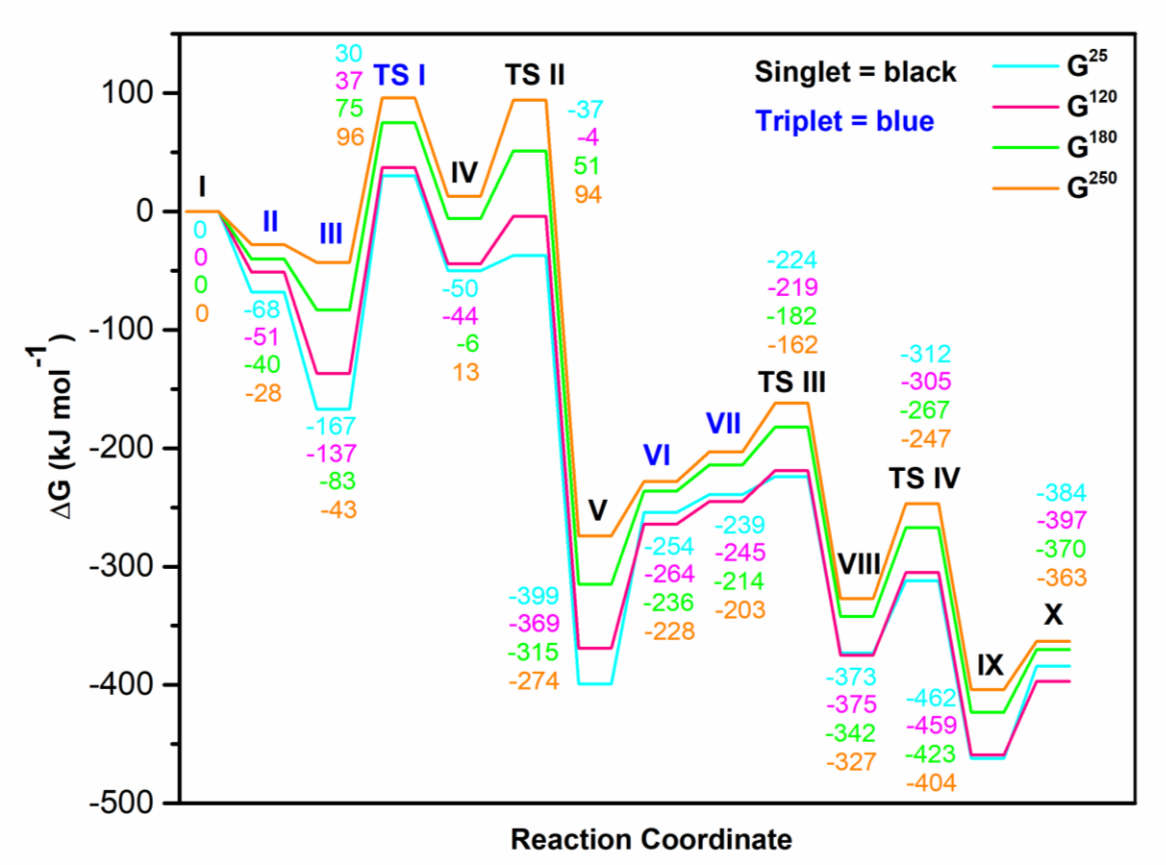

Figure S17. Gibbs free energy profile at the temperatures of 25, 120, 180 and 250 °C and 1 atm for the H_2 oxidation by O_2 on the Cu/UiO-66 catalyst.

<u>Related Discussion to data in Figure S18:</u>The comparision of relative Gibbs free energy (ΔG) at 25, 120, 180 and 250 °C reveals that both steps of H_2 oxidation are exergonic, similar to that the relative electronic energy (ΔE). Interestingly, the first transition state (TS I) emerges as the rate-determining step, which is in contrast to ΔE calculations, where the second transition state (TS II) was predicted to be the rate-determining step. Following the formation of intermediate IV, the reaction appears to progress towards TS II, leading to the formation of intermediate V. Notably, at 250 °C althrough the formation of intermeditate V seems more energetically favorable than H_2/O_2 co-adsorptioon (III), the calculated Gibbs free energies for the backward step (83 kJ/mol from IV to III via TSI) is very close to that for the forward step (81 kJ/mol from IV to V via TSII).

This near equal energy barrier slows down H_2 oxidation, in line with experimental observations discussed in section 3.2 of the main manuscript.

The Gibbs free energy profile also reveals that the adsorption of second H_2 molecule (intermediate VII) is energy-consuming, suggesting the weak adsorption ability of the Cu^{2+} sites for H_2. Furthermore, with increasing temperature the calculated ΔG for the second H_2 oxidation become less favorable (-462, -459, -423, and -404 kJ/mol for 25, 120, 180 and 250 °C, respectively). Overall, this computational result suggests the significant effect of temperature on the activity of Cu/UiO-66 catalsyt for H_2 oxidation, wiht higher reaction temperatures leading to reduced activity.

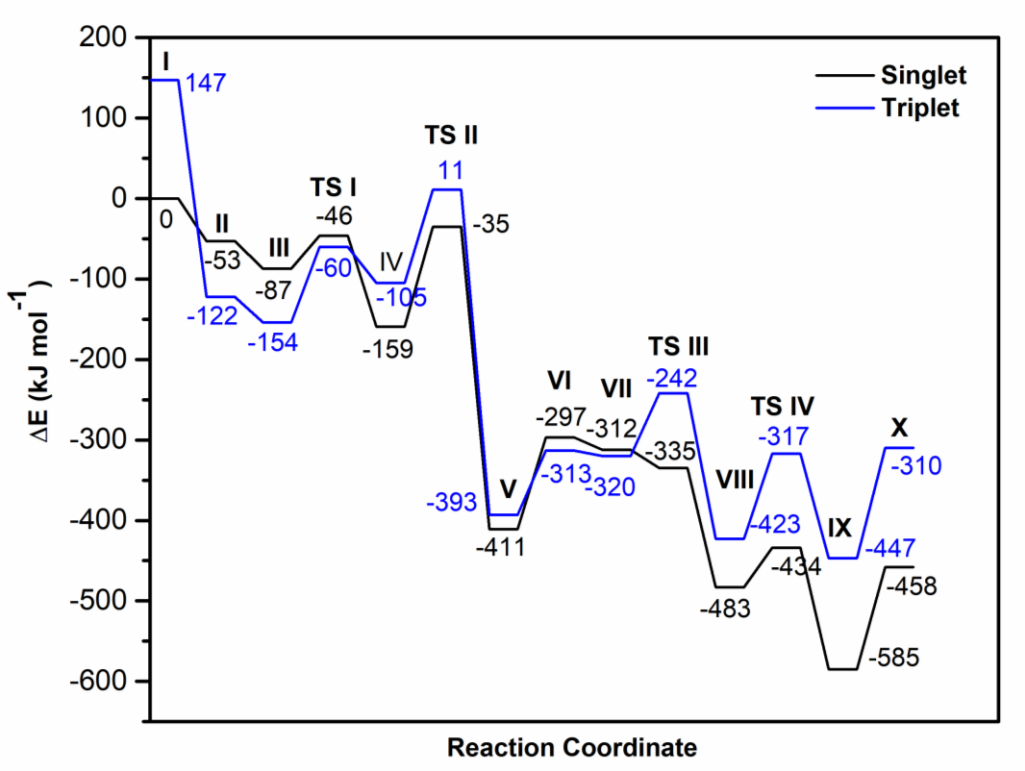

Figure S18. Energy profile for H_2 oxidation by O_2 on the Cu/UiO-66 model catalyst. The inserted values are the relative energies (ΔE).

In our study, we considered singlet and triplet spin states. Our calculations showed that the singlet state is the ground spin state for Cu^{1+} (intermediate **I**) with the triplet state being 147 kJ/mol higher in energy. During the reaction, spin state changes occurred. Following O_2 adsorption, the spin state changed from singlet to triplet and then returned to singlet after the first transition state **TS I**. During the first H_2 oxidation step (intermediate **VI**), a spin state change from singlet to triplet occurred, suggesting the oxidation of Cu^{1+} to Cu^{2+}. Then the spin state returned to singlet for the second H_2 oxidation step (from TS III to X), signifying the change in the oxidation state of Cu active site from +2 to +1.

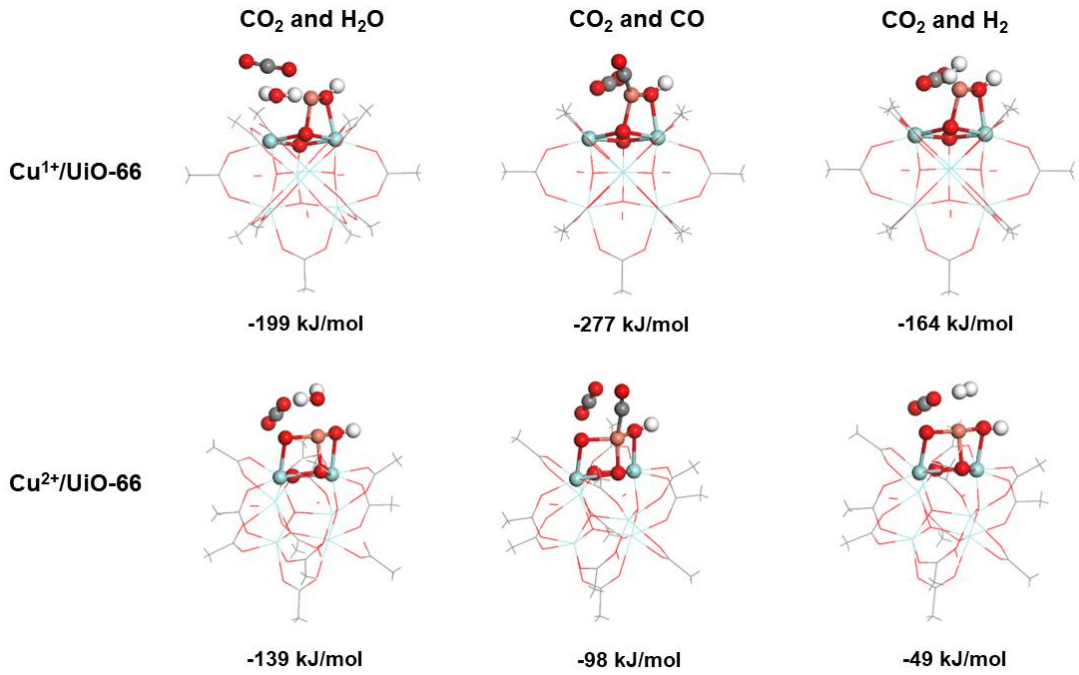

Figure S19. The optimized structures of the most stable co-adsorption of CO_2/H_2O, CO_2/CO and CO_2/H_2 on the Cu^{1+} and Cu^{2+} sites.